Characterizing the response of charge-couple device digital color cameras

Viktor Slavkovikj[a], Jon Yngve Hardeberg[a] and Alexander Eichhorn[b]

[a]Gjøvik University College, Teknologivegen 22, 2815 Gjøvik, Norway;

[b]Simula Research Laboratory, Martin Linges vei 17, 1364 Fornebu, Norway

ABSTRACT

The advance and rapid development of electronic imaging technology has lead the way to production of imaging sensors capable of acquiring good quality digital images with a high resolution. At the same time the cost and size of imaging devices have reduced. This has incited an increasing research interest for techniques that use images obtained by multiple camera arrays. The use of multi-camera arrays is attractive because it allows capturing multi-view images of dynamic scenes, enabling the creation of novel computer vision and computer graphics applications, as well as next generation video and television systems. There are additional challenges when using a multi-camera array, however. Due to inconsistencies in the fabrication process of imaging sensors and filters, multi-camera arrays exhibit inter-camera color response variations. In this work we characterize and compare the response of two digital color cameras, which have a light sensor based on the charge-coupled device (CCD) array architecture. The results of the response characterization process can be used to model the cameras' responses, which is an important step when constructing a multi-camera array system.

Keywords: CCD cameras, imaging sensors, spectral sensitivity curves, inter-camera color response variations, multi-camera arrays.

1. INTRODUCTION

Images obtained from a multi-camera array are used in a variety of computer vision and computer graphics applications. In the work of De Aguiar et al.[1] an array of eight cameras is used to perform marker-less reconstruction of a human performance scene. A circular dome camera system is used in the work of Li et al.[2] for the estimation of shapes and motions of 3D scenes without the aid of markers. Lou et al.[3] develop a real-time interactive multi-view video system which provides viewers with services such as view switching, frozen moment view, and view sweeping. Multiview camera configurations are used in methods for novel view rendering from virtual cameras for the purpose of free-viewpoint television.[4,5] In the work of Dumont et al.,[6] and Waizenegger and Feldman,[7] 3D teleconferencing systems are introduced which utilize camera arrays and virtual view synthesis[6] or 3D models of the captured scene[7] to enable immersive and natural communication in videoconferencing.

In distinct multi-camera array applications acquired images are used in different ways, such as combining entire images or applying computational methods on a subset of camera images. Nevertheless, all of these approaches suffer from performance degradation, which is due to inter-camera color response variations inherent to camera arrays for which the response of the individual cameras has not been established and adjusted for. The following sections describe the process of color response characterization for our experimental system.

Further author information:

[a]: E-mail: {viktor.slavkovikj, jon.hardeberg}@hig.no

[b]: E-mail: echa@ulrik.uio.no

Sensors, Cameras, and Systems for Industrial and Scientific Applications XIII,
edited by Ralf Widenhorn, Valérie Nguyen, Antoine Dupret, Proc. of SPIE-IS&T Electronic Imaging,
SPIE Vol. 8298, 82980G · © 2012 SPIE-IS&T · CCC code: 0277-786X/12/$18 · doi: 10.1117/12.909298

2. MODELING THE CAMERAS' RESPONSE FUNCTIONS

The light sensors used in many solid state cameras are based on CCD readout technology.[8] Charge-coupled devices exhibit linear intensity-response functions over a wide operating range; however, the overall camera system might not have the underlying device linearity.[9,10] It is, therefore, necessary to characterize the response of the system, and, if needed, correct the output data for any non-linearity. It is important to evaluate the camera response so that:

- The camera response to a constant stimulus is known as a function of exposure time.
- The camera response is known as a function of variable light intensity.

We have designed and conducted two different measurement procedures, described in Sec. 2.1 and 2.2, intended to enable us model the cameras' response functions. Two Basler Pilot digital color cameras, model piA1900-32gc, were used in the measurements. The CCD array architecture of the light sensor used in this camera model is shown in Figure 1. This is an interline transfer architecture, where the photo-sensitive elements (pixels) are

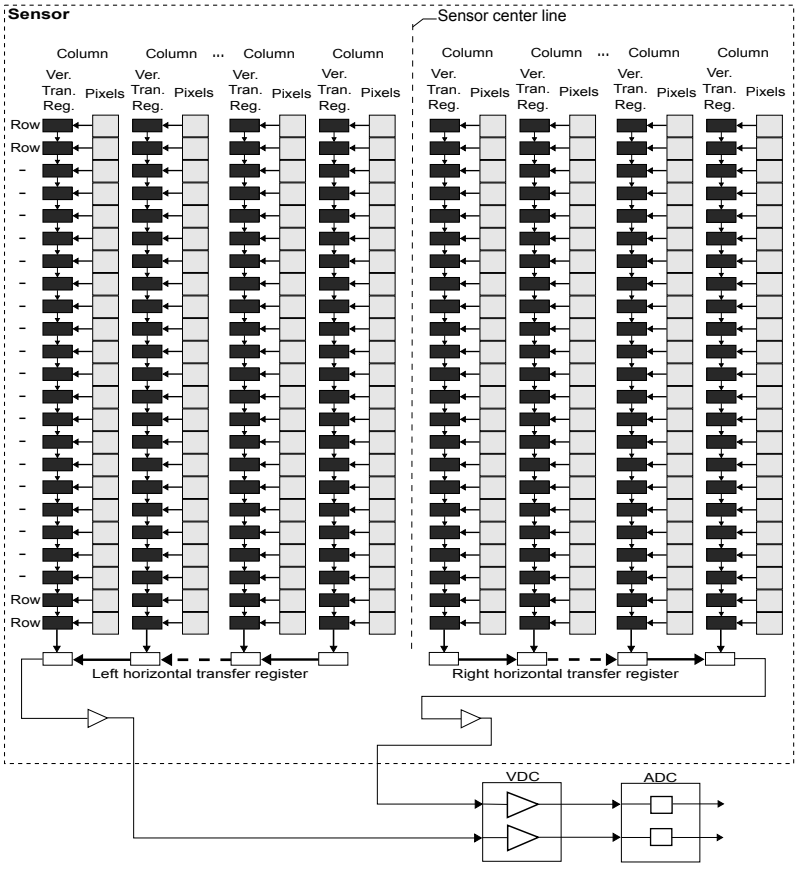

Figure 1. Diagram of the light sensor CCD architecture.

separated by vertical transfer registers. The transfer registers are shielded by an opaque metal cover to prevent smear during the readout process. After the integration time has elapsed, the electrical charge generated at each location of the pixels is transferred to the vertical transfer registers. A progressive scan approach is used, so that the entire image is captured in a given moment of time. After the charges have been transferred to the vertical transfer registers the last row of the vertical transfer registers is moved to the two horizontal transfer registers, as shown in Figure 1. In this particular design, the sensor array is divided into two parts. Charges from the right half of the sensor are transferred to the right horizontal transfer register, and charges from the left half of the sensor are transferred to the left horizontal transfer register. Charges moving out of the horizontal

transfer registers are converted to voltages, proportional to the size of each charge. A variable gain controller VGC is then used to amplify each voltage. The amplified signal is finally digitized by the 12 bit analog-to-digital converter ADC.

2.1 Measuring Cameras' Spectral Sensitivities

The intrinsic color quality of the images taken with a given camera depends on the spectral characteristics of the camera's imaging sensor.[10,11] In addition to this, the difference in sensors' spectral characteristics is the main cause for inter-camera color response variations.

The basic experimental procedure was to measure the spectral sensitivity curves for the cameras in our system by exposing each camera to narrow band illumination. To gain insight on how the exposure time influences the sensitivities of the camera, we repeated the measurements for different fixed camera exposure times, obtaining the spectral sensitivity curves for each of the predefined camera exposures.

A monochromator device (Bentham TMc300) was used to produce the narrow band illumination. This monochromator is a Czerny-Turner type of a monochromator design (see Figure 2), where the light A from the monochromator internal light source is focused on the entrance slit B to be collimated by a curved mirror C. The collimated light then impinges on a grating D where it is diffracted. The dispersed light is then re-focused by a mirror E at the exit slit F. The grating D is rotatable, and the angle of the grating determines which wavelengths of light would pass through the exit slit F. The narrow band light from the exit slit is passed through

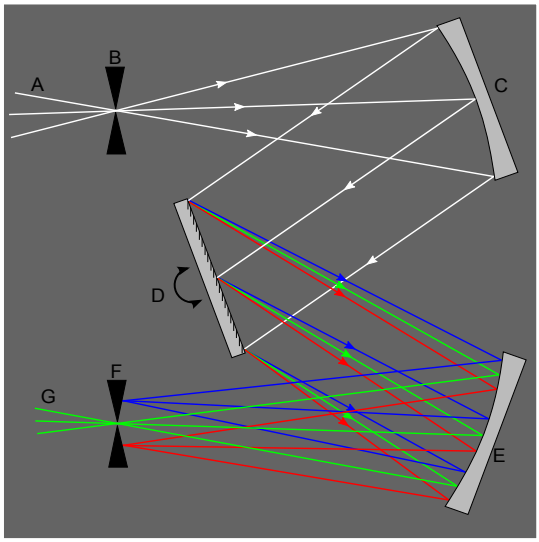

Figure 2. Diagram of a Czerny-Turner monochromator design.

the entrance opening of an integrating sphere. The integrating sphere's exit aperture then acts as a narrow band light source of uniform radiance. The full width at half maximum FWHM of the wavelength distribution passed by the exit slit i.e. the spectral bandpass BP depends on the width W of the slit and the reciprocal linear dispersion R_d, which depends on the grating, as follows:

$$BP = W \times R_d. \tag{1}$$

By adjusting the width of the slit we set the bandpass at approximately 1 nm.

We place the camera so that the exit of the integrating sphere is in focus. The aperture size is fixed to $f/1.4$, and all of the automatic image processing functions have been turned off. Using the monochromator we change the wavelength of the light from 380 nm to 780 nm in 1 nm steps. For each wavelength we take twenty captures with the camera, averaging a 100×100 pixels rectangular patch from the image center. We used the sensor's Bayer pattern image to obtain the average response from the pixels overlaid with red, green, and blue filter accordingly. To estimate the mean value of the additive dark current noise, images with the lens cap on

the camera were taken. For camera 1 we measured the spectral sensitivity curves for exposure times given in the following sequence of exposure durations: 1 ms, 2 ms, 3 ms, 4 ms, 5 ms, 6 ms, 7 ms, 8 ms, 9 ms, 10 ms, 20 ms, 30 ms, 40 ms, 50 ms, 60 ms, 70 ms, 80 ms, 90 ms, and 100 ms. For camera 2 spectral sensitivity curves were measured for a subset of the previous exposure durations i.e. for: 1 ms, 5 ms, 10 ms, 50 ms, and 100 ms exposures. Figure 3 shows a joint plot of the spectral sensitivities for camera 1 and camera 2, for 100 ms exposure time, where the result are scaled with the same values. The difference between the spectral sensitivity for each of the color channels is clearly visible here. It has to be considered, when analyzing the spectral sensitivity curves,

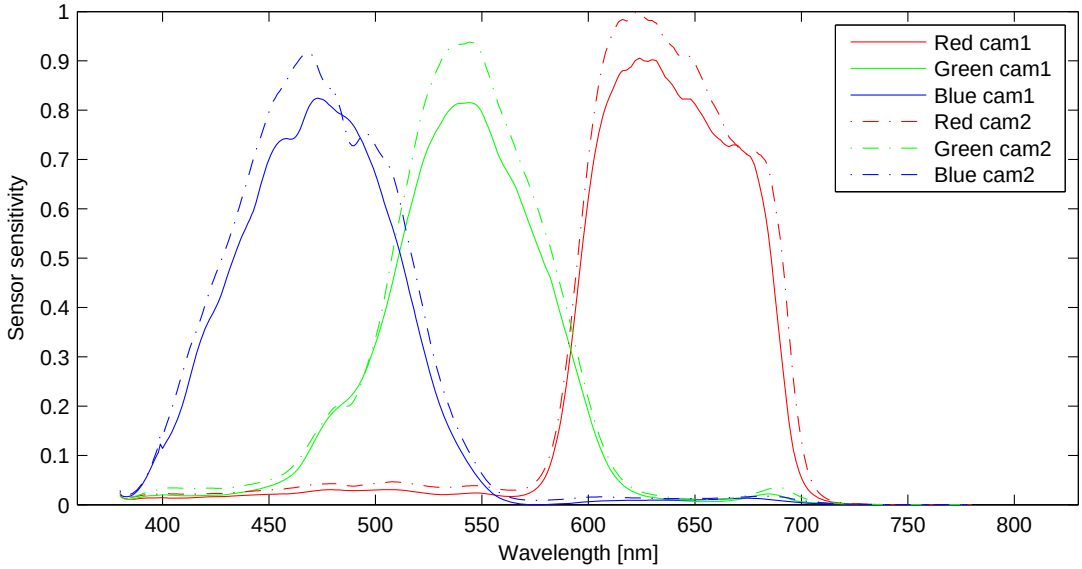

Figure 3. Spectral sensitivity curves, camera 1 solid lines, camera 2 dot-dash lines (exposure time 100 ms).

that the cameras have a cut filter in front of the sensors, which transmits in the range of around 400 nm to around 700 nm.[12]

An original measurement, i.e. the response of the i_{th} sensor $D_i(\lambda)$ to a monochromatic wavelength λ, is the product of the monochromator illuminant spectral radiance $S(\lambda)$ and the sensor spectral sensitivity $q_i(\lambda)$, as given in Equation (2)

$$D_i(\lambda) = S(\lambda)q_i(\lambda) + \eta_i\,, \tag{2}$$

where $i \in \{R, G, B\}$, and η_i is the noise term. Note that the sensor spectral sensitivity term $q_i(\lambda)$ represents the spectral sensitivities of both the detector (pixel) and its overlaid filter. For a given wavelength λ, the sensor sensitivity $q_i(\lambda)$ is the quotient of the division of the difference between the sensor response $D_i(\lambda)$ and the expected value of the noise η_i with the monochromator illuminant radiance $S(\lambda)$. The spectral radiance of the monochromator illuminant was measured with a spectroradiometer (Minolta CS-1000) for the wavelength interval 380 nm to 780 nm and 2 nm step, and the measurements were interpolated to obtain data with 1 nm step.

If we select fixed wavelengths from the red, green, and blue parts of the spectrum and plot the measured sensor sensitivities for all of the different exposure times, we obtain the graphs shown in Figure 4 and Figure 5 for camera 1 and camera 2 respectively. The calculated Pearson correlation coefficients between the original measured data and the fitted lines, shown in Figure 4 and Figure 5, are given in table 1. From the obtained results we can conclude that the cameras' responses are linear with regard to exposure time in the interval of exposure times in which the measurements were made.

We calculate the uncertainties of the measurements of the sensors' spectral sensitivity curves. Note that the sensor spectral sensitivity is a derived quantity. Considering Equation (2), the sensor spectral sensitivity $q_i(\lambda)$ is

$$q_i(\lambda) = \frac{D_i(\lambda)}{S(\lambda)} - \frac{\eta_i}{S(\lambda)}. \tag{3}$$

Table 1. Correlation coefficients of measured and fitted data from Figure 4 and Figure 5.

Correlation Coefficients			
Channels	Red	Green	Blue
Camera 1	1.0000	1.0000	0.9999
Camera 2	1.0000	1.0000	0.9998

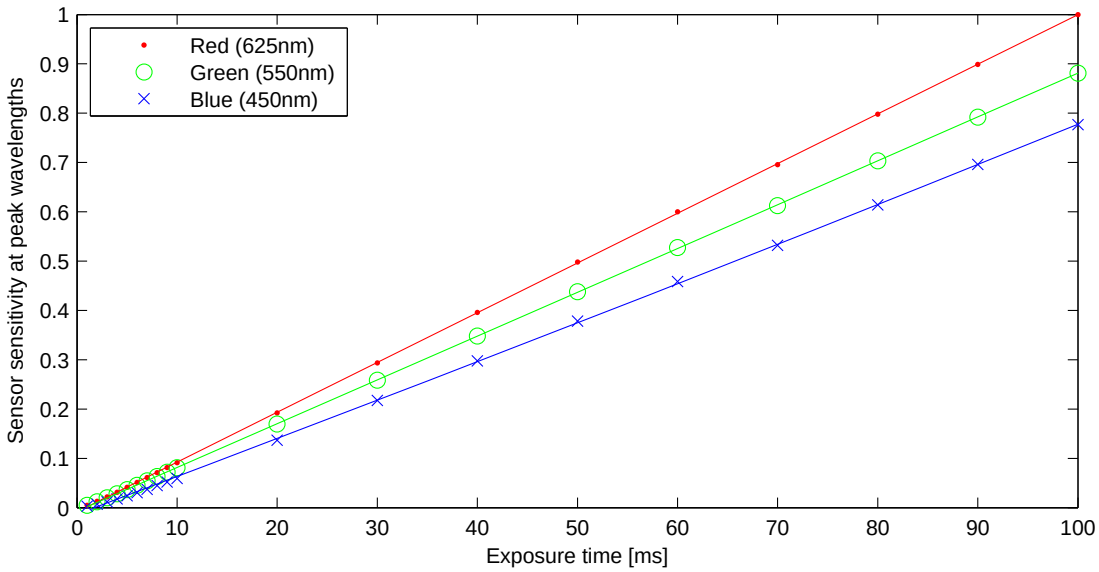

Figure 4. Sensor sensitivity at peak wavelengths as a function of exposure time (camera 1).

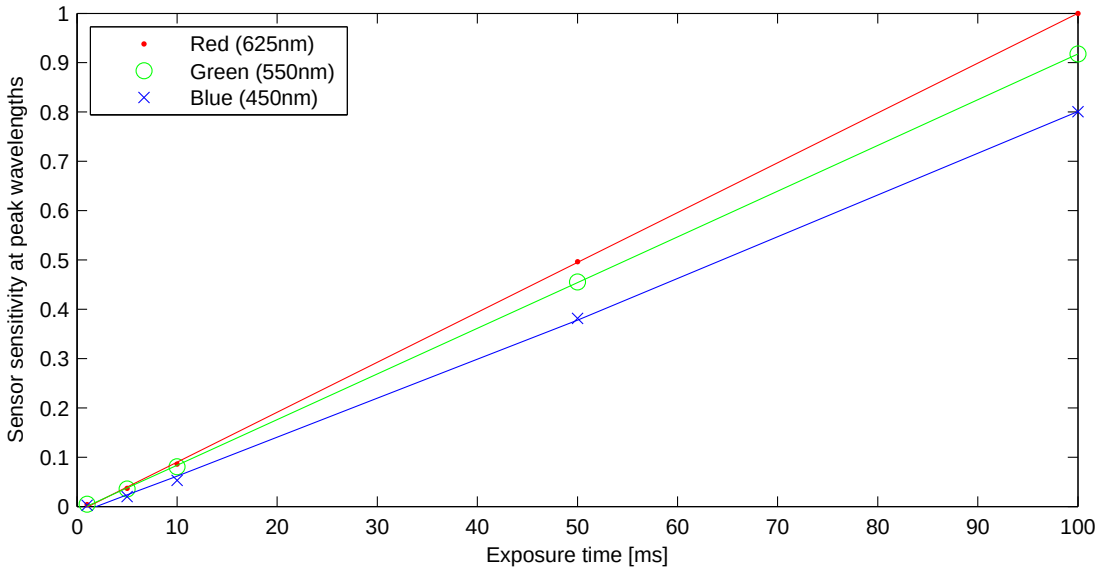

Figure 5. Sensor sensitivity at peak wavelengths as a function of exposure time (camera 2).

From Equation (3) we can derive the relation between the measured values and their uncertainties, and the uncertainty of the spectral sensitivity $\Delta q_i(\lambda)$ as

$$\Delta q_i(\lambda) = \sqrt{\frac{S^2(\lambda)(\Delta D_i^2(\lambda) + \Delta \eta_i^2) + \Delta S^2(\lambda)(D_i^2(\lambda) + \eta_i^2)}{S^4(\lambda)}}\,, \tag{4}$$

where for a given wavelength λ, $\Delta D_i(\lambda)$ denotes the uncertainty of the measured camera response, $\Delta\eta_i$ is the uncertainty of the noise, and $\Delta S(\lambda)$ is the uncertainty of the monochromator illuminant spectral radiance measurement. The expected values along with the uncertainties of the spectral sensitivity curves for both cameras, for exposure times of 100 ms, are given in tables 4 and 5 in Appendix A. For brevity only data from every twentieth measurement are shown in tables 4 and 5.

2.2 Measuring cameras' responses to variable light intensities

We measure next the response of the cameras for varying levels of light intensities. For this purpose we place the camera focusing the medium gray background of a light booth. The lens aperture size is fixed to f/1.4, and all of the camera's automatic image processing functions have been turned off. The light booth reproduces CIE illuminant D50, and the intensity of the light can be varied, using the light booth's control, from two to one hundred relative units in steps of two relative units. For every light intensity level we capture twenty frames with the camera, averaging a rectangular region of interest of 200×160 pixels from the image center. The sensor's Bayer pattern image was used to get the corresponding average response of the pixels overlaid with a red, green, and a blue filter. Frames with the lens cap on the camera were taken to estimate the mean value of the dark noise. A standard white reference tile was placed in the light booth. We consider the perfect reflecting diffuser as a secondary light source and, by placing a spectroradiometer (Minolta CS-1000) next to the camera at approximately the same distance from the light booth, we measure its integrated radiance in the visible range, from 380 nm to 780 nm in 1nm steps. This is done sequentially, for every intensity level, after acquiring the images with the camera. Considering Lambertian conditions, if radiant intensity is needed, it could be calculated by the product of the radiance and the surface of the secondary source. For each measurement series the camera's exposure duration is kept fixed. We also made measurement series for the following exposure durations: 0.1 ms. 0.2 ms, 0.3 ms, 0.4 ms, 0.5 ms, 0.6 ms, 0.7 ms, 0.8 ms, 0.9 ms, 1 ms, 2 ms, 3 ms, 4 ms, 5 ms, 6 ms, 7 ms, 8 ms, 9 ms, 10 ms, 20 ms, 30 ms, and 40 ms. All of the measurements, as was done for the measurements of the sensors' spectral sensitivity curves described in the previous section, were done in a dark room minimizing the possible sources of stray radiation.

Figure 6 and Figure 7 show a plot, for camera 1 and camera 2 respectively, of the scaled sensor response as a function of increasing radiance. The measurements plotted in Figure 6 and Figure 7 are for exposure time of 7 ms. The expected values of the measurements in digital counts, used to produce the plots in Figure 6 and

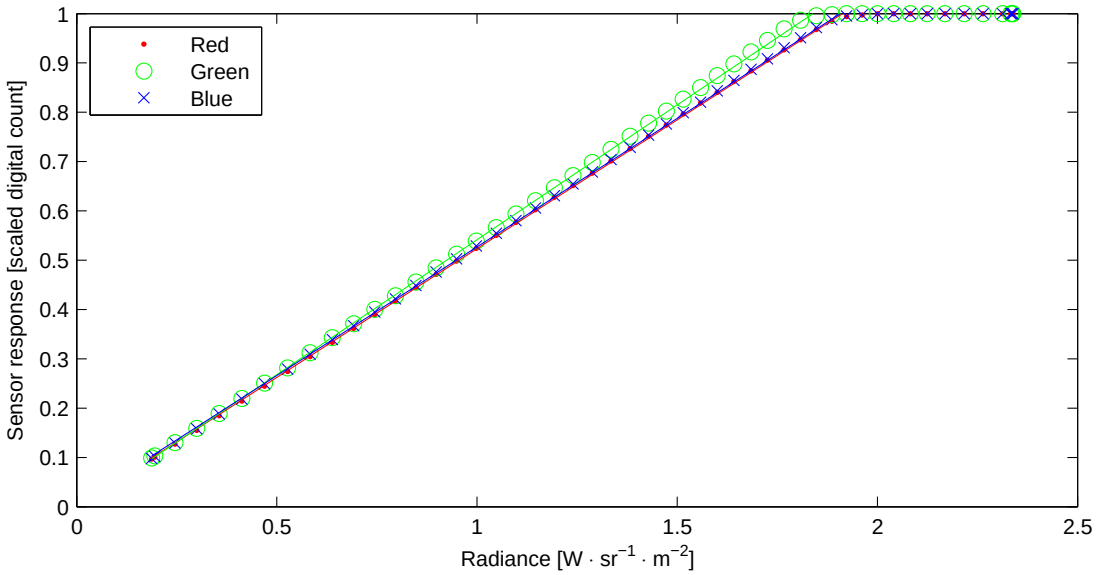

Figure 6. Sensor response as a function of radiance (camera 1, 7 ms exposure time).

Figure 7, together with the uncertainties of the measurement data are given in appendix B in table 6 and table 7

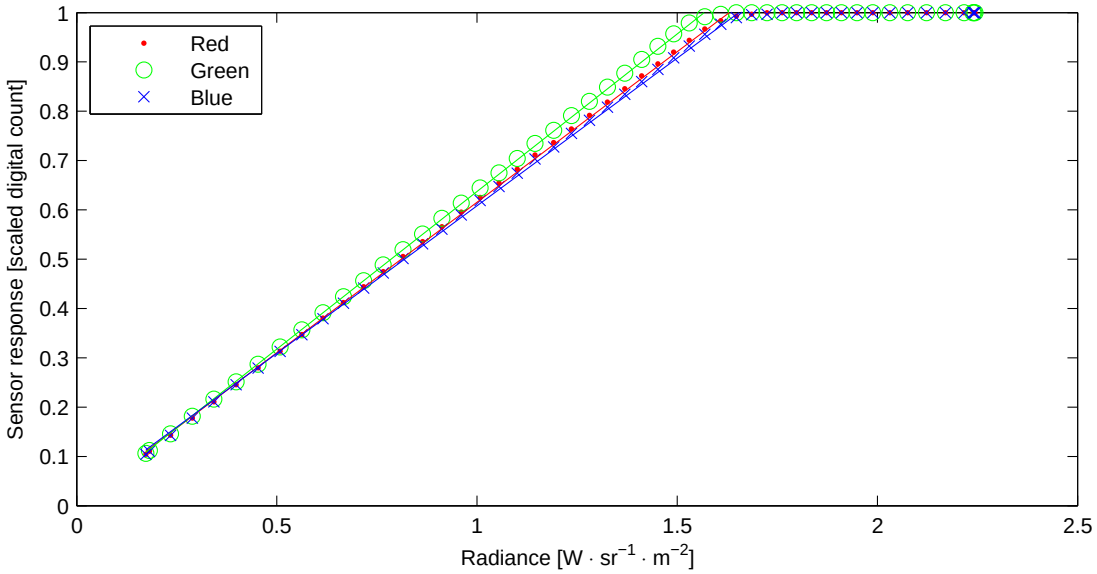

Figure 7. Sensor response as a function of radiance (camera 2, 7 ms exposure time).

respectively. Also note that the presented data contain some measurements for radiance magnitudes for which the cameras' sensors saturate. We calculate the correlation coefficients between the original measurements, where no sensor saturation occurs, and the fitted lines to the data, as shown in Figure 6 and Figure 7. The results are shown in table 2.

Table 2. Correlation coefficients of measured and fitted data from Figure 6 and Figure 7.

Correlation Coefficients			
Channels	Red	Green	Blue
Camera 1	0.9998	0.9998	0.9998
Camera 2	0.9996	0.9998	0.9994

We can obtain the variation of the gain for each color channel as a function of the exposure duration, if we plot the slope of the fitted lines for each of the sensor response measurements, for varying radiance, with regards to the exposure time of the measurements. The graphs, for camera 1 and camera 2, are shown in Figure 8 and Figure 9 respectively. The results show that the responses of the cameras' sensors exhibit good linearity, with regard to variable intensity of the detected light, in the range in which the measurements were made.

Table 3. Correlation coefficients of lines fitted to the data from Figure 8 and Figure 9.

Correlation Coefficients			
Channels	Red	Green	Blue
Camera 1	1.0000	0.9999	1.0000
Camera 2	0.9997	0.9982	0.9998

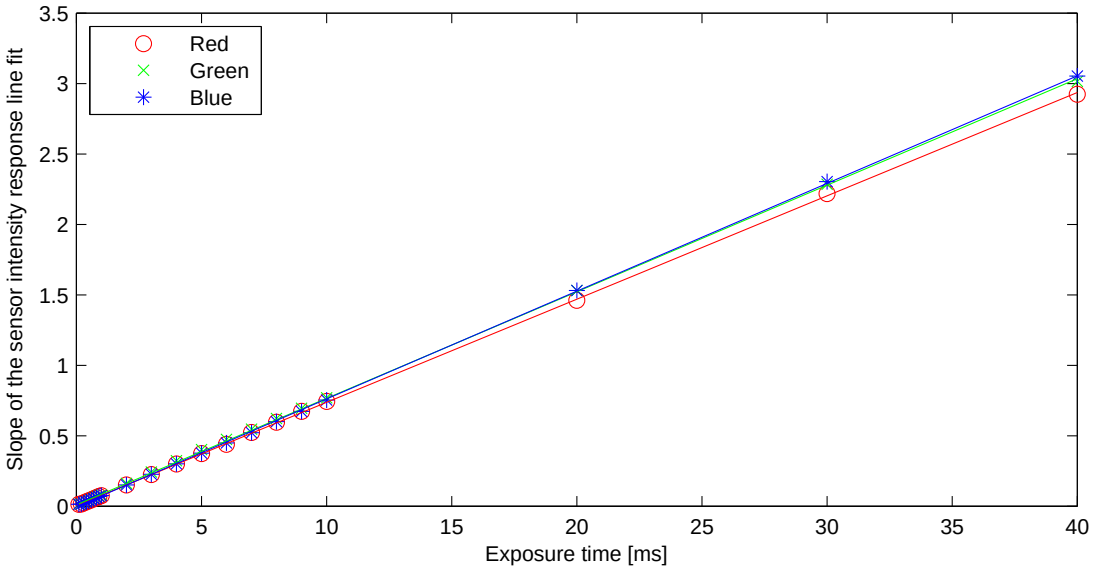

Figure 8. Variation of gain as a function of exposure time (camera 1).

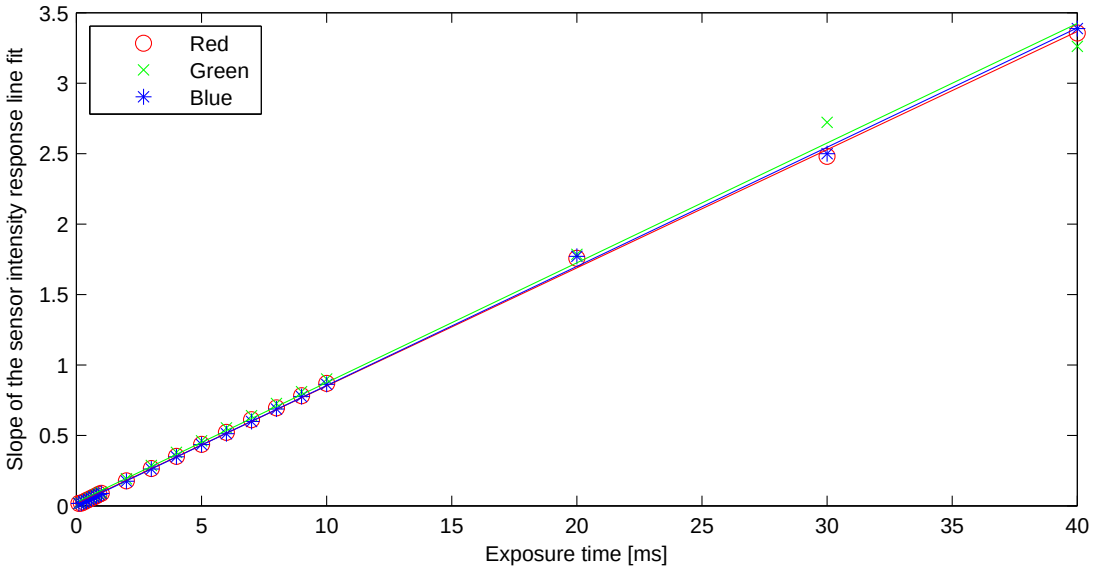

Figure 9. Variation of gain as a function of exposure time (camera 2).

3. CAMERA RESPONSE MODEL

Considering the results from the previous sections, the camera response model can be given by Equation (5)

$$R_i = g \int_{\lambda_l}^{\lambda_h} S(\lambda) q_i(\lambda)\, \mathrm{d}\lambda + \eta_i\,, \tag{5}$$

where $S(\lambda)$ at wavelength λ is the radiance incident to the sensor, $q_i(\lambda)$ is the spectral sensitivity of the sensor pixel covered with the i_{th} filter type, $i \in \{R,\ G,\ B\}$, and η_i represent the mean of the dark noise of the i_{th} sensor. The term g given in Equation (5) represents the gain, and is a linear function $\mathbb{R} \longrightarrow \mathbb{R}$ of the exposure time e

$$g = f(e). \tag{6}$$

The upper and lower wavelength limits are denoted as λ_l and λ_h respectively.

4. SUMMARY

The spectral sensitivities of the sensor of a digital color camera play an important role in determining the color characteristics of the device. While detail characterization of the response of a camera may be of lesser significance in applications where only one camera is used to acquire images, it is important for applications where multi-view images, obtained from a multiple camera array, are used. We have investigated the response of two CCD-based digital color cameras, under varying exposure times, light intensity levels, and for narrow band and broad band light stimuli, and used the result from the measurements to model the cameras' response. From our measurements we can conclude that even for cameras of the same type and series of production, under equal parameter settings, the color response cannot be considered the same. Since the difference in sensors spectral characteristics are the main cause for inter-camera response variations it is necessary to verify any assumptions about cameras' responses. In this work we have shown a way to obtain a detailed characterization of cameras' response, which can provide a greater control when trying to obtain a consistent inter-camera response from a multi-camera array.

APPENDIX A. SPECTRAL SENSITIVITY CURVES, EXPECTED VALUES AND UNCERTAINTIES

Table 4: Spectral sensitivity curves for camera 1, expected values and uncertainties of measured data in absolute units (exposure time 100 ms).

$\lambda\ [nm]$	$q_R(\lambda) \pm \Delta q_R(\lambda)\ [\frac{DC \cdot sr \cdot m^2}{W}]$	$q_G(\lambda) \pm \Delta q_G(\lambda)\ [\frac{DC \cdot sr \cdot m^2}{W}]$	$q_B(\lambda) \pm \Delta q_B(\lambda)\ [\frac{DC \cdot sr \cdot m^2}{W}]$
380	$(4.79 \pm 0.70) \times 10^3$	$(4.34 \pm 0.48) \times 10^3$	$(5.62 \pm 0.69) \times 10^3$
400	$(3.54 \pm 0.13) \times 10^3$	$(5.01 \pm 0.10) \times 10^3$	$(28.35 \pm 0.16) \times 10^3$
420	$(3.88 \pm 0.08) \times 10^3$	$(4.68 \pm 0.07) \times 10^3$	$(88.44 \pm 0.17) \times 10^3$
440	$(4.77 \pm 0.07) \times 10^3$	$(6.70 \pm 0.05) \times 10^3$	$(141.21 \pm 0.16) \times 10^3$
460	$(5.53 \pm 0.05) \times 10^3$	$(14.29 \pm 0.04) \times 10^3$	$(183.73 \pm 0.17) \times 10^3$
480	$(7.52 \pm 0.03) \times 10^3$	$(46.35 \pm 0.04) \times 10^3$	$(199.42 \pm 0.13) \times 10^3$
500	$(7.46 \pm 0.03) \times 10^3$	$(80.87 \pm 0.05) \times 10^3$	$(166.00 \pm 0.09) \times 10^3$
520	$(6.26 \pm 0.02) \times 10^3$	$(163.59 \pm 0.07) \times 10^3$	$(89.36 \pm 0.05) \times 10^3$
540	$(5.51 \pm 0.02) \times 10^3$	$(201.71 \pm 0.09) \times 10^3$	$(27.15 \pm 0.03) \times 10^3$
560	$(4.37 \pm 0.02) \times 10^3$	$(170.70 \pm 0.07) \times 10^3$	$(2.51 \pm 0.02) \times 10^3$
580	$(14.72 \pm 0.02) \times 10^3$	$(119.11 \pm 0.05) \times 10^3$	$(0.08 \pm 0.02) \times 10^3$
600	$(154.45 \pm 0.07) \times 10^3$	$(46.52 \pm 0.02) \times 10^3$	$(1.53 \pm 0.02) \times 10^3$
620	$(219.98 \pm 0.09) \times 10^3$	$(7.06 \pm 0.02) \times 10^3$	$(2.21 \pm 0.02) \times 10^3$

Continued on next page

Table 4 – continued from previous page

$\lambda\ [nm]$	$q_R(\lambda) \pm \Delta q_R(\lambda)\ [\frac{DC \cdot sr \cdot m^2}{W}]$	$q_G(\lambda) \pm \Delta q_G(\lambda)\ [\frac{DC \cdot sr \cdot m^2}{W}]$	$q_B(\lambda) \pm \Delta q_B(\lambda)\ [\frac{DC \cdot sr \cdot m^2}{W}]$
640	$(210.17 \pm 0.09) \times 10^3$	$(2.32 \pm 0.01) \times 10^3$	$(2.27 \pm 0.02) \times 10^3$
660	$(185.04 \pm 0.09) \times 10^3$	$(1.58 \pm 0.01) \times 10^3$	$(2.67 \pm 0.02) \times 10^3$
680	$(162.18 \pm 0.07) \times 10^3$	$(4.79 \pm 0.01) \times 10^3$	$(3.11 \pm 0.02) \times 10^3$
700	$(13.57 \pm 0.02) \times 10^3$	$(1.52 \pm 0.01) \times 10^3$	$(0.97 \pm 0.02) \times 10^3$
720	$(0.59 \pm 0.03) \times 10^3$	$(0.30 \pm 0.02) \times 10^3$	$(0.23 \pm 0.02) \times 10^3$
740	$(0.08 \pm 0.02) \times 10^3$	$(0.05 \pm 0.02) \times 10^3$	$(0.05 \pm 0.03) \times 10^3$
760	$(0.05 \pm 0.02) \times 10^3$	$(0.04 \pm 0.02) \times 10^3$	$(0.03 \pm 0.03) \times 10^3$
780	$(0.04 \pm 0.04) \times 10^3$	$(0.03 \pm 0.03) \times 10^3$	$(0.03 \pm 0.04) \times 10^3$

Table 5: Spectral sensitivity curves for camera 2, expected values and uncertainties of measured data in absolute units (exposure time 100 ms).

$\lambda\ [nm]$	$q_R(\lambda) \pm \Delta q_R(\lambda)\ [\frac{DC \cdot sr \cdot m^2}{W}]$	$q_G(\lambda) \pm \Delta q_G(\lambda)\ [\frac{DC \cdot sr \cdot m^2}{W}]$	$q_B(\lambda) \pm \Delta q_B(\lambda)[\frac{DC \cdot sr \cdot m^2}{W}]$
380	$(6.50 \pm 0.92) \times 10^3$	$(5.76 \pm 0.66) \times 10^3$	$(7.13 \pm 0.93) \times 10^3$
400	$(5.68 \pm 0.17) \times 10^3$	$(8.30 \pm 0.13) \times 10^3$	$(34.21 \pm 0.20) \times 10^3$
420	$(5.53 \pm 0.11) \times 10^3$	$(8.34 \pm 0.09) \times 10^3$	$(100.39 \pm 0.18) \times 10^3$
440	$(6.64 \pm 0.07) \times 10^3$	$(9.96 \pm 0.05) \times 10^3$	$(163.98 \pm 0.19) \times 10^3$
460	$(8.33 \pm 0.06) \times 10^3$	$(18.02 \pm 0.05) \times 10^3$	$(216.70 \pm 0.19) \times 10^3$
480	$(10.58 \pm 0.04) \times 10^3$	$(48.25 \pm 0.04) \times 10^3$	$(208.25 \pm 0.14) \times 10^3$
500	$(10.61 \pm 0.04) \times 10^3$	$(83.60 \pm 0.05) \times 10^3$	$(180.47 \pm 0.10) \times 10^3$
520	$(10.03 \pm 0.04) \times 10^3$	$(188.08 \pm 0.09) \times 10^3$	$(110.36 \pm 0.06) \times 10^3$
540	$(9.13 \pm 0.03) \times 10^3$	$(231.35 \pm 0.10) \times 10^3$	$(34.96 \pm 0.05) \times 10^3$
560	$(7.58 \pm 0.03) \times 10^3$	$(194.88 \pm 0.08) \times 10^3$	$(5.04 \pm 0.03) \times 10^3$
580	$(19.18 \pm 0.36) \times 10^3$	$(135.84 \pm 0.59) \times 10^3$	$(2.30 \pm 0.03) \times 10^3$
600	$(174.06 \pm 0.08) \times 10^3$	$(53.27 \pm 0.03) \times 10^3$	$(3.78 \pm 0.03) \times 10^3$
620	$(244.20 \pm 0.10) \times 10^3$	$(8.86 \pm 0.02) \times 10^3$	$(3.45 \pm 0.03) \times 10^3$
640	$(229.81 \pm 0.09) \times 10^3$	$(3.55 \pm 0.02) \times 10^3$	$(3.08 \pm 0.03) \times 10^3$
660	$(198.97 \pm 0.39) \times 10^3$	$(2.73 \pm 0.02) \times 10^3$	$(3.31 \pm 0.03) \times 10^3$
680	$(176.19 \pm 0.08) \times 10^3$	$(6.32 \pm 0.02) \times 10^3$	$(4.27 \pm 0.03) \times 10^3$
700	$(32.09 \pm 0.04) \times 10^3$	$(3.78 \pm 0.02) \times 10^3$	$(2.19 \pm 0.03) \times 10^3$
720	$(0.86 \pm 0.03) \times 10^3$	$(0.50 \pm 0.02) \times 10^3$	$(0.44 \pm 0.03) \times 10^3$
740	$(0.12 \pm 0.03) \times 10^3$	$(0.10 \pm 0.02) \times 10^3$	$(0.10 \pm 0.03) \times 10^3$
760	$(0.04 \pm 0.03) \times 10^3$	$(0.04 \pm 0.02) \times 10^3$	$(0.04 \pm 0.03) \times 10^3$
780	$(0.05 \pm 0.05) \times 10^3$	$(0.04 \pm 0.04) \times 10^3$	$(0.04 \pm 0.06) \times 10^3$

APPENDIX B. SENSOR RESPONSE FOR VARYING RADIANCE, EXPECTED VALUES AND UNCERTAINTIES

Table 6: Sensor responses for varying radiance, expected values and uncertainties of measured data in absolute units (camera 1, 7 ms exposure time).

$L_e\ [W \cdot sr^{-1} \cdot m^{-2}]$	$R \pm \Delta R\ [DC]$	$G \pm \Delta G\ [DC]$	$B \pm \Delta B\ [DC]$
0.1872	396.40 ± 0.49	405.53 ± 1.41	401.95 ± 2.07
0.1949	412.70 ± 0.49	422.22 ± 1.45	418.46 ± 2.06
0.2455	520.01 ± 0.69	532.16 ± 1.86	529.07 ± 2.42
0.2998	634.43 ± 0.83	649.98 ± 2.35	646.99 ± 3.10
0.3558	755.11 ± 0.81	774.48 ± 2.52	770.06 ± 3.62
0.4128	876.62 ± 1.08	899.80 ± 2.83	894.23 ± 3.93
0.4695	1000.99 ± 0.91	1027.86 ± 2.94	1020.67 ± 4.12
0.5273	1123.27 ± 1.06	1153.19 ± 2.93	1143.31 ± 4.21
0.5833	1246.06 ± 1.23	1279.46 ± 3.53	1267.02 ± 4.94
0.6384	1365.61 ± 1.08	1403.02 ± 3.76	1388.58 ± 5.31
0.6919	1480.21 ± 1.18	1520.58 ± 4.01	1503.43 ± 5.51
0.7444	1596.11 ± 1.45	1638.88 ± 4.33	1617.10 ± 6.13
0.7960	1706.85 ± 1.56	1752.78 ± 4.29	1726.87 ± 6.21
0.8474	1818.59 ± 1.88	1867.42 ± 5.18	1837.63 ± 7.01
0.8980	1929.76 ± 1.86	1983.38 ± 5.18	1950.33 ± 7.16
0.9489	2039.44 ± 1.98	2096.94 ± 5.49	2059.38 ± 7.59
0.9982	2145.98 ± 1.51	2207.12 ± 5.41	2165.22 ± 7.51
1.0484	2253.69 ± 1.85	2318.58 ± 5.86	2270.77 ± 8.03
1.0971	2361.97 ± 2.30	2430.79 ± 6.27	2376.33 ± 8.60
1.1462	2467.32 ± 2.21	2541.29 ± 6.25	2481.50 ± 8.41
1.1932	2569.89 ± 1.76	2649.03 ± 6.36	2583.58 ± 8.95
1.2397	2666.84 ± 2.21	2751.27 ± 6.83	2679.82 ± 9.58
1.2880	2770.50 ± 2.16	2859.94 ± 6.82	2780.79 ± 9.37
1.3349	2871.98 ± 2.94	2968.33 ± 7.81	2883.67 ± 10.46
1.3825	2973.80 ± 2.36	3077.10 ± 7.61	2984.25 ± 10.39
1.4285	3075.35 ± 2.52	3185.91 ± 8.33	3086.62 ± 11.29
1.4731	3169.92 ± 2.91	3285.46 ± 8.33	3178.01 ± 11.43
1.5150	3260.88 ± 2.44	3385.62 ± 8.49	3272.28 ± 11.25
1.5586	3351.33 ± 2.94	3481.21 ± 8.87	3359.97 ± 11.53
1.5997	3440.57 ± 2.71	3581.07 ± 9.08	3453.59 ± 12.07
1.6416	3530.42 ± 2.71	3676.72 ± 9.20	3540.43 ± 12.45
1.6841	3620.11 ± 3.17	3776.29 ± 10.67	3632.35 ± 14.25
1.7252	3707.55 ± 3.36	3872.51 ± 11.16	3720.32 ± 14.69
1.7672	3794.65 ± 3.13	3969.03 ± 10.06	3811.45 ± 14.44
1.8081	3879.05 ± 3.78	4041.40 ± 6.66	3894.96 ± 14.61
1.8474	3962.64 ± 3.67	4077.99 ± 2.28	3979.48 ± 15.15
1.8863	4031.35 ± 2.14	4086.04 ± 0.30	4043.81 ± 9.96
1.9231	4070.92 ± 1.22	4095.00 ± 0.08	4075.94 ± 3.90

Continued on next page

Table 6 – continued from previous page

$L_e\ [W \cdot sr^{-1} \cdot m^{-2}]$	$D_R \pm \Delta D_R\ [DC]$	$D_G \pm \Delta D_G\ [DC]$	$D_B \pm \Delta D_B\ [DC]$
1.9616	4083.51 ± 0.23	4095.00 ± 0.08	4084.26 ± 0.60
2.0003	4095.00 ± 0.03	4095.00 ± 0.08	4095.00 ± 0.16
2.0405	4095.00 ± 0.00	4095.00 ± 0.08	4095.00 ± 0.16
2.0823	4095.00 ± 0.00	4095.00 ± 0.08	4095.00 ± 0.16
2.1243	4095.00 ± 0.00	4095.00 ± 0.08	4095.00 ± 0.16
2.1690	4095.00 ± 0.00	4095.00 ± 0.08	4095.00 ± 0.16
2.2169	4095.00 ± 0.00	4095.00 ± 0.08	4095.00 ± 0.16
2.2639	4095.00 ± 0.00	4095.00 ± 0.08	4095.00 ± 0.16
2.3125	4095.00 ± 0.00	4095.00 ± 0.08	4095.00 ± 0.16
2.3333	4095.00 ± 0.00	4095.00 ± 0.08	4095.00 ± 0.16
2.3360	4095.00 ± 0.00	4095.00 ± 0.08	4095.00 ± 0.16
2.3386	4095.00 ± 0.00	4095.00 ± 0.08	4095.00 ± 0.16

Table 7: Sensor responses for varying radiance, expected values and uncertainties of measured data in absolute units (camera 2, 7 ms exposure time).

$L_e\ [W \cdot sr^{-1} \cdot m^{-2}]$	$D_R \pm \Delta D_R\ [DC]$	$D_G \pm \Delta D_G\ [DC]$	$D_B \pm \Delta D_B\ [DC]$
0.1731	427.88 ± 0.54	433.88 ± 1.52	426.69 ± 2.21
0.1816	452.96 ± 0.55	459.14 ± 1.57	450.51 ± 2.24
0.2343	586.64 ± 0.94	597.31 ± 2.37	584.99 ± 3.30
0.2891	728.19 ± 0.70	742.98 ± 2.28	727.38 ± 2.92
0.3427	863.38 ± 0.84	884.33 ± 2.53	863.18 ± 3.58
0.3980	1004.81 ± 0.75	1028.37 ± 3.01	1004.03 ± 4.06
0.4533	1145.28 ± 1.20	1173.76 ± 3.59	1143.78 ± 4.94
0.5080	1284.16 ± 1.04	1317.92 ± 3.24	1281.10 ± 4.32
0.5624	1422.38 ± 1.44	1461.45 ± 3.87	1419.78 ± 5.36
0.6154	1558.56 ± 1.45	1602.50 ± 4.40	1552.66 ± 6.16
0.6662	1687.88 ± 1.77	1736.13 ± 4.55	1681.53 ± 6.33
0.7167	1818.79 ± 1.51	1868.85 ± 4.88	1807.26 ± 6.98
0.7658	1944.51 ± 1.35	1999.29 ± 4.74	1932.44 ± 6.72
0.8151	2068.96 ± 2.44	2126.64 ± 6.11	2052.67 ± 8.14
0.8641	2193.57 ± 2.12	2256.29 ± 6.32	2174.91 ± 8.62
0.9120	2316.53 ± 1.66	2386.30 ± 6.04	2297.13 ± 8.04
0.9606	2439.56 ± 1.84	2512.91 ± 6.18	2415.35 ± 8.45
1.0078	2561.05 ± 2.60	2639.58 ± 6.96	2533.77 ± 9.37
1.0549	2681.02 ± 1.93	2764.34 ± 6.81	2651.10 ± 9.63
1.1003	2795.73 ± 2.23	2883.23 ± 6.84	2762.32 ± 9.49
1.1450	2912.46 ± 2.34	3008.15 ± 7.34	2879.44 ± 9.84
1.1912	3016.91 ± 2.30	3118.30 ± 7.62	2979.54 ± 10.19
1.2359	3129.83 ± 2.12	3239.25 ± 8.18	3091.15 ± 11.19

Continued on next page

Table 7 – continued from previous page

$L_e\ [W \cdot sr^{-1} \cdot m^{-2}]$	$R \pm \Delta R\ [DC]$	$G \pm \Delta G\ [DC]$	$B \pm \Delta B\ [DC]$
1.2811	3242.15 ± 2.55	3358.14 ± 8.54	3201.61 ± 11.43
1.3259	3351.86 ± 1.89	3475.06 ± 7.91	3309.35 ± 10.80
1.3693	3463.86 ± 2.96	3592.80 ± 8.48	3417.65 ± 11.28
1.4112	3569.50 ± 2.55	3705.94 ± 9.05	3522.16 ± 11.82
1.4516	3669.47 ± 2.74	3814.75 ± 9.81	3622.77 ± 13.16
1.4912	3768.32 ± 3.13	3919.11 ± 9.90	3718.67 ± 14.17
1.5301	3865.40 ± 3.35	4009.08 ± 7.29	3818.14 ± 14.42
1.5687	3958.46 ± 3.19	4061.71 ± 3.58	3914.22 ± 13.91
1.6088	4027.45 ± 2.26	4081.56 ± 0.83	3998.03 ± 11.35
1.6478	4067.18 ± 0.91	4095.00 ± 0.02	4053.02 ± 5.88
1.6859	4080.99 ± 0.24	4095.00 ± 0.00	4077.69 ± 1.91
1.7241	4095.00 ± 0.02	4095.00 ± 0.00	4082.06 ± 0.14
1.7621	4095.00 ± 0.00	4095.00 ± 0.00	4095.00 ± 0.01
1.7980	4095.00 ± 0.00	4095.00 ± 0.00	4095.00 ± 0.01
1.8359	4095.00 ± 0.00	4095.00 ± 0.00	4095.00 ± 0.00
1.8732	4095.00 ± 0.00	4095.00 ± 0.00	4095.00 ± 0.00
1.9102	4095.00 ± 0.00	4095.00 ± 0.00	4095.00 ± 0.00
1.9492	4095.00 ± 0.00	4095.00 ± 0.00	4095.00 ± 0.00
1.9886	4095.00 ± 0.00	4095.00 ± 0.00	4095.00 ± 0.00
2.0314	4095.00 ± 0.00	4095.00 ± 0.00	4095.00 ± 0.00
2.0757	4095.00 ± 0.00	4095.00 ± 0.00	4095.00 ± 0.00
2.1226	4095.00 ± 0.00	4095.00 ± 0.00	4095.00 ± 0.00
2.1698	4095.00 ± 0.00	4095.00 ± 0.00	4095.00 ± 0.00
2.2165	4095.00 ± 0.00	4095.00 ± 0.00	4095.00 ± 0.00
2.2386	4095.00 ± 0.00	4095.00 ± 0.00	4095.00 ± 0.00
2.2410	4095.00 ± 0.00	4095.00 ± 0.00	4095.00 ± 0.00
2.2438	4095.00 ± 0.00	4095.00 ± 0.00	4095.00 ± 0.00

ACKNOWLEDGMENTS

This work was supported by the Norwegian Color Research Laboratory, Gjøvik, Norway, and by Simula Research Laboratory, Oslo, Norway.

REFERENCES

[1] de Aguiar, E., Stoll, C., Theobalt, C., Ahmed, N., Seidel, H.-P., and Thrun, S., "Performance Capture from Sparse Multi-view Video," in [*ACM SIGGRAPH 2008 papers*], *SIGGRAPH '08*, 98:1–98:10, ACM, New York, NY, USA (2008).

[2] Li, K., Dai, Q., and Xu, W., "Markerless Shape and Motion Capture From Multiview Video Sequences," *Circuits and Systems for Video Technology, IEEE Transactions on* **21**, 320–334 (March 2011).

[3] Lou, J.-G., Cai, H., and Li, J., "A Real-Time Interactive Multi-View Video System," in [*Proceedings of the 13th annual ACM international conference on Multimedia*], *MULTIMEDIA '05*, 161–170, ACM, New York, NY, USA (2005).

[4] Min, D. B., Kim, D., Yun, S., and Sohn, K., "2D/3D freeview video generation for 3DTV system," *Sig. Proc.: Image Comm.* **24**(1-2), 31–48 (2009).
[5] Mori, Y., Fukushima, N., Yendo, T., Fujii, T., and Tanimoto, M., "View generation with 3D warping using depth information for FTV," *Sig. Proc.: Image Comm.* **24**(1-2), 65–72 (2009).
[6] Dumont, M., Rogmans, S., Lafruit, G., and Bekaert, P., "Immersive Teleconferencing with Natural 3D Stereoscopic Eye Contact Using GPU Computing," in [*Proceedings of 3D Stereo Media*], (January 2010).
[7] Waizenegger, W. and Feldmann, I., "Calibration of a Synchronized Multi-camera Setup for 3D Videoconferencing," in [*3DTV-Conference: The True Vision - Capture, Transmission and Display of 3D Video (3DTV-CON)*], 1–4 (June 2010).
[8] Holst, G. C., [*CCD arrays, cameras, and displays*], JCD Pub. ; SPIE Optical Engineering, Winter Park, FL, 2nd ed. (1998).
[9] Vora, P. L., Farrell, J. E., Tietz, J. D., and Brainard, D. H., "Digital color cameras - 1 - Response models," tech. rep., Hewlett-Packard Company (March 1997).
[10] Vora, P. L., Farrell, J. E., Tietz, J. D., and Brainard, D. H., "Digital color cameras - 2 - Spectral Response," tech. rep., Hewlett-Packard Company (March 1997).
[11] Sharma, G. and Trussell, H. J., "Figures of Merit for Color Scanners," *IEEE Transactions on Image Processing* , 990–1001 (1997).
[12] Basler Vision Technologies, *Basler Pilot User's Manual for GigE Vision Cameras* (September 2008).